42nd AIAA Aerospace Sciences Meeting and Exhibit
5-8 January 2004, Reno, Nevada

AIAA 2004-653

AIAA 2004-0653

Computational Analysis on Nozzle Performance of a RP Laser Thruster

Y. Hirooka, H. Katsurayama, K. Mori,
K. Komurasaki and Y. Arakawa
The University of Tokyo
Tokyo, Japan

42nd Aerospace Sciences Meeting & Exhibit
5–8 January 2004
Reno, Nevada

Computational Analysis on Nozzle Performance of a RP Laser Thruster

Yasuro Hirooka*, Hiroshi Katsurayama†, Koichi Mori‡,
Kimiya Komurasaki§ and Yoshihiro Arakawa¶
The University of Tokyo, Hongo 7-3-1, Bunkyo, Tokyo 113-8656, Japan

Abstract

In order to develop a scaling law for a nozzle design of a repetitive pulsed (RP) laser thruster, momentum-coupling coefficients C_m were computed for several conical nozzle geometries by means of CFD. Especially, blast wave expansion and air refilling processes were analyzed. As a result, an optimum nozzle length was obtained. In addition, higher C_m was obtained with smaller apex angle. This is because a stronger expansion wave is induced due to smaller apex angle and the pressure inside of nozzle is lowered quickly. However, there found some discrepancies between the CFD predictions and measurements. This is partly because of the finite propagation period of a Laser Supported Detonation wave. To utilize the absorbed energy in the LSD process effectively, laser pulse width has to be short enough.

INTRODUCTION

One of the current serious problems in space development is the cost for payload delivery to space, and a RP laser thruster is attracting attention as a low-cost launching system recently. A RP laser thruster is free from on-board energy sources because laser beam is transmitted from laser bases on the earth or space. In addition, it can use the ambient atmosphere as a propellant. Thereby, a RP laser thruster will increase its payload ratio drastically in comparison with conventional chemical rockets.

Input laser energy E_i is converted to impulsive thrust I through the sequential processes (a)-(d) shown in Fig. 1. The plasma produced by laser focusing absorbs the input laser energy in the form of a Laser Supported Detonation (LSD) wave (a). The LSD wave expands explosively and drives a strong blast wave (b). The blast wave imparts an impulse directly to the nozzle wall and is accelerated aerodynamically through the nozzle (c). Finally, air is refilled from the nozzle exit (d).

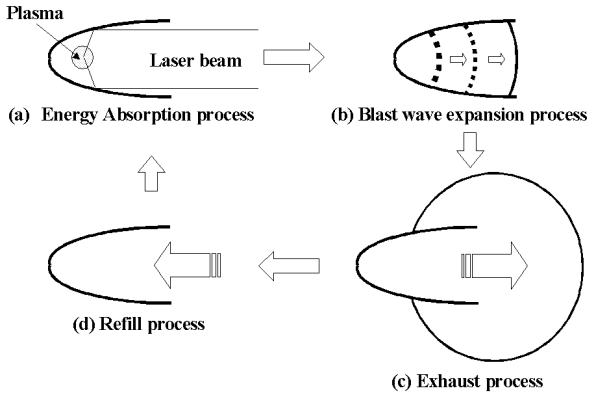

Fig. 1 Conversion processes from E_i to I

In the process (b), the absorbed energy is converted to blast wave energy E_{bw}, chemical potential energy and radiation energy. E_{bw} is defined as,

$$E_{bw} = \int [\rho e^{t+r}(T) + \frac{\rho(u^2+v^2)}{2} - \rho_0 e^{t+r}(T_0)]dV \ , \quad (1)$$

where

$$\rho e^{t+r} = \sum_{s=1}^{11} \rho_s \left[\int C_V^s(T)dT - \int C_{V,V}^s(T)dT - \Delta e_s^f \right]. \quad (2)$$

The subscript 0 indicates the properties before laser incidence and s indicates species. ρ is density, e^{t+r} is the sum of translational and rotational energies, T is static temperature, u and v are axial and radial

---

* Graduate student, Department of Aeronautics and Astronautics
† Graduate student, Department of Aeronautics and Astronautics, Student Member AIAA
‡ Graduate student, Department of Advanced Energy, Student Member AIAA
§ Associate Professor, Department of Advanced Energy, Member AIAA
¶ Professor, Department of Aeronautics and Astronautics, Member AIAA

velocity components respectively, C^s_V is specific heat at constant volume for species s, $C^s_{V,V}$ is specific heat at constant volume for species s for vibrational energy, and Δe^f is chemical potential energy.

The blast wave efficiency η_{bw}, is defined as,

$$\eta_{bw} = \frac{E_{bw}}{E_i}. \quad (3)$$

Its dependencies on focusing f-number, input energy and ambient pressure have been discussed in our previous researches.[1, 2)]

In the processes (c) and (d), E_{bw} is converted to I by the nozzle. Therefore, the clarification of these processes is indispensable to predict the performance of a RP laser thruster. However, it is impossible to apply the conventional nozzle theory with steady flow, because the flow field inside of the nozzle is essentially unsteady.

In this study, the propagations of blast waves inside and outside of nozzles were solved by CFD to investigate the influence of the exhaust-refill process on momentum-coupling coefficient C_m ($=I/E_i$). Conical nozzles were adapted as a representative shape because of their simple configurations.

COMPUTATIONAL METHOD

Non-dimensional nozzle length

The non-dimensional nozzle length r [2)] is defined as,

$$r = \frac{R_n}{R^*}, \quad (4)$$

where R_n is an actual nozzle length. R^* is a characteristic radius of shock wave defined as,

$$R^* = \left(\frac{2E_{bw}}{p_a(1-\cos\alpha_d)} \right)^{\frac{1}{3}}, \quad (5)$$

where p_a is an ambient air pressure and α_d is a half apex angle of conical nozzle. R^* is a measure of the strength of explosion and equivalent to the radius of the shock wave when the post-shock pressure decays to p_a.

Governing equations

Axisymmetric Navier-Stokes equations are solved. Air is treated as an ideal gas. Then, the governing equations are given by

$$\frac{\partial \mathbf{U}}{\partial t} + \frac{\partial \mathbf{F}}{\partial z} + \frac{1}{r}\frac{\partial r\mathbf{G}}{\partial r} = \frac{\partial \mathbf{F_v}}{\partial z} + \frac{1}{r}\frac{\partial r\mathbf{G_v}}{\partial r} + \frac{\mathbf{H}}{r}, \quad (6)$$

Table 1 Nozzle configurations

(a) r dependency

α_d, degrees	15		
R_n, mm	30.9	58.0	77.3
Nozzle exit radius, mm	8	15	20
E_i, J	11		
η_{bw}, %	44		
r	0.219	0.411	0.548

(b) α_d dependency

α_d, degrees	10	40	70
R_n, mm	72.0	28.9	20.5
Nozzle exit radius, mm	12.5	18.6	19.2
E_i, J	10		
η_{bw}, %	44		
r	0.402		

$$\mathbf{U} = \begin{bmatrix} \rho \\ \rho u \\ \rho v \\ E \end{bmatrix}, \mathbf{F} = \begin{bmatrix} \rho u \\ \rho u^2 + p \\ \rho uv \\ (E+p)u \end{bmatrix}, \mathbf{G} = \begin{bmatrix} \rho v \\ \rho uv \\ \rho v^2 + p \\ (E+p)v \end{bmatrix},$$

$$\mathbf{F_v} = \begin{bmatrix} 0 \\ \tau_{zz} \\ \tau_{zr} \\ u\tau_{zz} + v\tau_{zr} + q_z \end{bmatrix}, \mathbf{G_v} = \begin{bmatrix} 0 \\ \tau_{zr} \\ \tau_{rr} \\ u\tau_{zr} + v\tau_{rr} + q_r \end{bmatrix},$$

$$\mathbf{H} = \begin{bmatrix} 0 \\ 0 \\ p - \tau_{\theta\theta} \\ 0 \end{bmatrix}. \quad (7)$$

E and the equation of state are defined as

$$E = \rho C_p T - p + \frac{\rho(u^2+v^2)}{2}, \quad (8)$$

$$p = \rho RT, \quad (9)$$

$$C_p = \frac{\gamma}{\gamma - 1} R. \quad (10)$$

Herein, specific heat ratio γ is 1.4 and gas constant of air R is 287 J/(kgK). Transport properties are estimated using Southerland's equation.

Numerical Scheme

A cell-centered finite difference scheme is adopted. Inviscid flux is estimated with the AUSM-DV scheme[3)] and space accuracy is extended to 3rd-order by the MUSCL approach with Edwards's pressure limiter[4)]. Viscous flux is estimated with a standard central difference. Time integration is

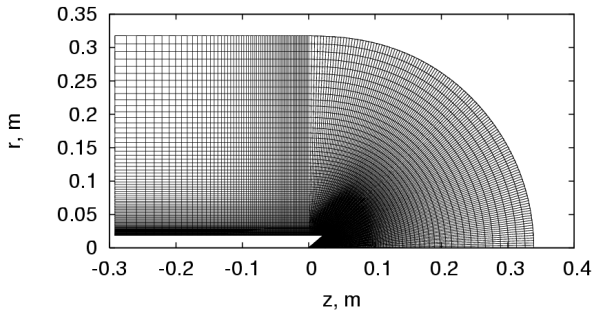

Fig. 2 Computational mesh
(α_d = 40°, r = 0.402, 40,668 cells)

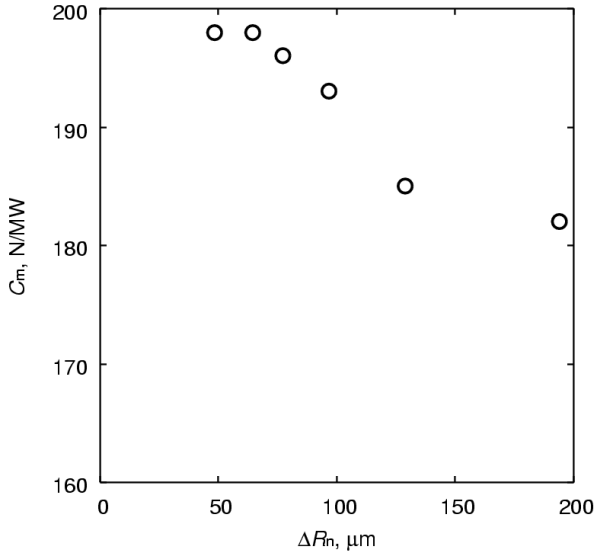

Fig. 3 Mesh convergence (α_d =50°, r = 0.394)

performed with the LU-SGS scheme[5] that is extended to 3rd-order time accuracy by Matsuno's inner iteration method[6]. The calculation is performed with the CFL number of 1.5-300.

To investigate the conversion from E_{bw} to I, r and α_d tabulated in Table 1 are taken as parameters. Twelve deferent nozzle lengths are tested for α_d = 15° and 50°, and seven angles for r = 0.402.

In all calculations, blast waves are driven in the standard quiescent atmosphere.

Computational mesh

Figure 2 shows computational meshes of a conical nozzle and the surrounding region. The mesh of inside of the nozzle is fine enough to correctly capture the propagation of the blast wave.

The outer boundary of the computational zone is set far from the nozzle to reduce the influence of non-physical reflection waves.

Mesh convergence is shown in Fig. 3. Convergence was obtained at $\Delta R_n < 100\mu$m. Then the mesh with $\Delta R_n = 100\mu$m is used in the following calculations. The number of cells is about 40,000.

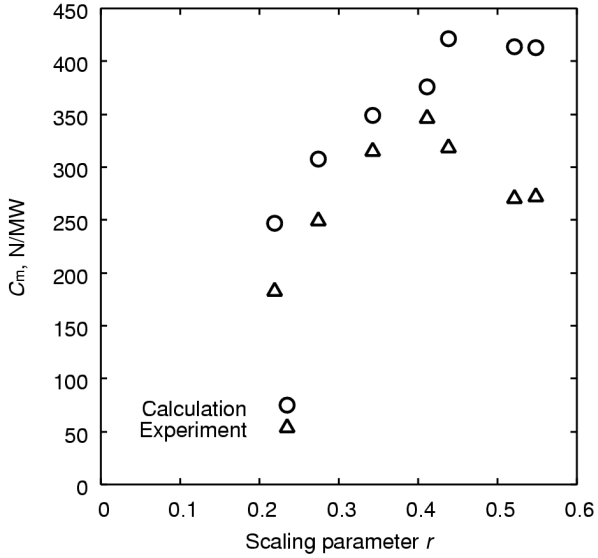

Fig. 4 Influence of nozzle length on C_m (α_d =15°)

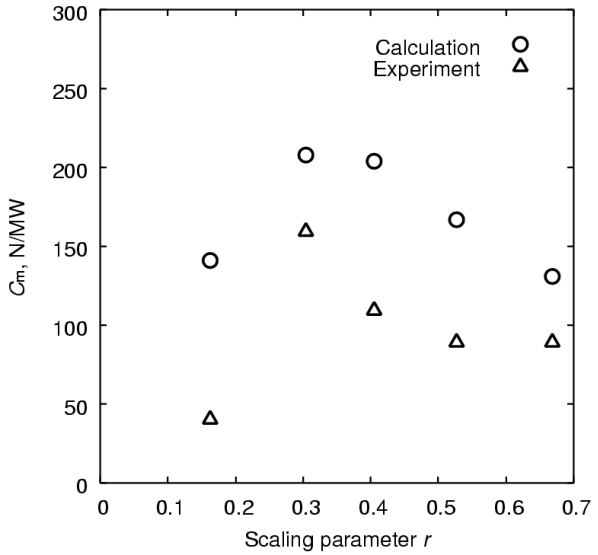

Fig. 5 Influence of nozzle length on C_m (α_d = 50°)

Explosion source model

An explosion source model[7] is adopted instead of solving the LSD phenomenon using a thermo-chemically non-equilibrium model. The explosion source is modeled as a pressurized volume. Because the LSD heating process is isometric,[8] the density in the source is assumed to be equal to an ambient atmosphere.

In this paper, an explosion source is assumed to be a sphere. Its initial radius is set to 1 mm. η_{bw} is taken from the experimental data[1] as η_{bw} = 0.44. Both η_{bw} and E_{bw} are assumed to be invariant during the blast wave propagation process.

The source is set in the vicinity of cone apex. In the case of α_d=10°, it is at 4.76 mm downstream of

the apex.

RESULTS AND DISCUSSIONS

Optimum nozzle length

Figures 4 and 5 show the correlation between C_m and r. The experimental data are taken from Ref. 2. As shown in Fig. 4, C_m increases with r as far as $r <$ 0.4 in both CFD and the experiment for $\alpha_d = 15°$. In r > 0.4, CFD overestimates C_m. The reason for this discrepancy is not clear now.

For α_d=50°, C_m has a peak at r = 0.3 in CFD and the experiment as seen in Fig. 5. However, CFD overestimates C_m by 30~200%.

In conclusion, the optimum nozzle length would be 0.3~0.4R^*. This correlation has been predicted theoretically in Ref. 2.

C_m dependency on α_d

Figure 6 shows the C_m dependency on α_d. r was fixed to 0.402. As shown in the figure, C_m decreases with α_d, while the tendency is more drastic in the experiment than in CFD. These reason will be discussed in the following sessions.

The results obtained here can be applied to various nozzle configurations since α_d is equivalent to the aspect ratio of a general nozzle.

Histories of thrust and C_m

Figure 7 shows the thrust history of α_d = 10° and r = 0.402. The thrust decreases drastically until t_1, when shock wave reaches nozzle exit. The thrust is kept to be positive until t_2, and then decreases to negative. The recovery from negative thrust starts at t_3, and the thrust again returns to positive at t_4. The shock front propagates very far from the nozzle exit at this time. After this time, the thrust periodically oscillates on zero thrust. Its oscillation attenuates gradually.

Figure 8 shows the history of C_m for r = 0.402. Its horizontal axis denotes normalized time t^*, defined as,

$$t^* = \frac{t}{t_1}, \qquad (11)$$

where t is time and t_1 is the same in Fig. 7. t_1 is about 48 μs for α_d =10°, 20 μs for 40° and 13 μs for 70° respectively. Hence the time scale of α_d = 10° is 3.7 times as long as that of α_d = 70°.

In any α_d, C_m reaches its maximum value at the same normalized time, $t^*_2 \cong 1.9t^*_1$. However, after t^*_2, the history of C_m is strongly dependent on α_d. The

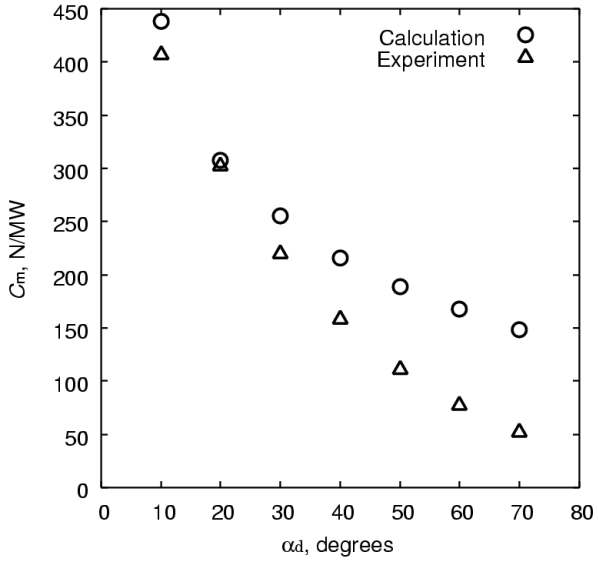

Fig. 6 Influence of α_d on C_m (r = 0.402)

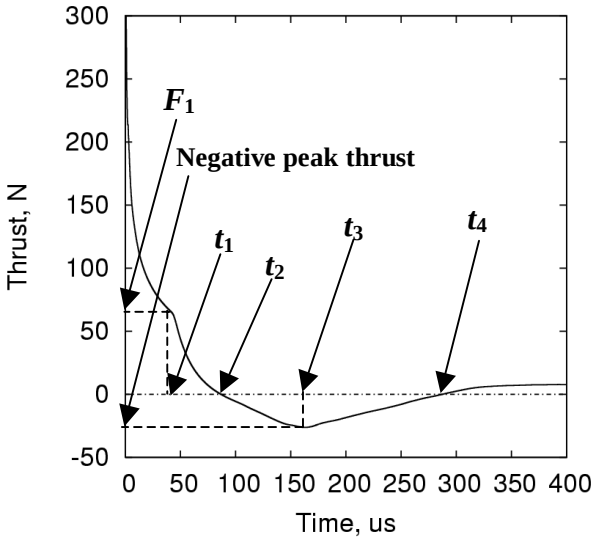

Fig. 7 History of thrust (α_d = 10°, r = 0.402)

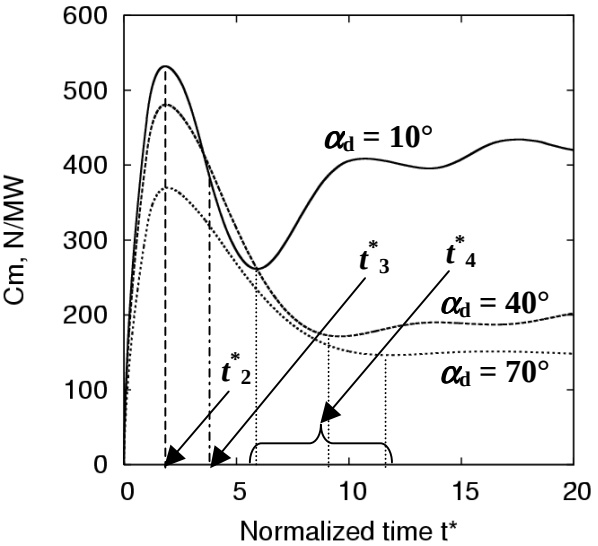

Fig. 8 History of C_m (r = 0.412)

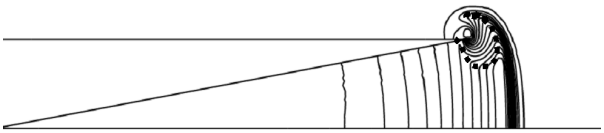

(a) 58 μs (t^* = 1.21)
(P_{max} = 3.45 atm, P_{min} = 0.659 atm, dP = 0.186 atm)

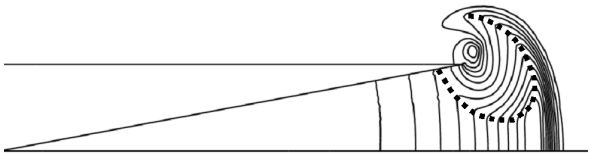

(b) 68 μs (t^* = 1.42)
(P_{max} = 2.95 atm, P_{min} = 0.480 atm, dP = 0.164 atm)

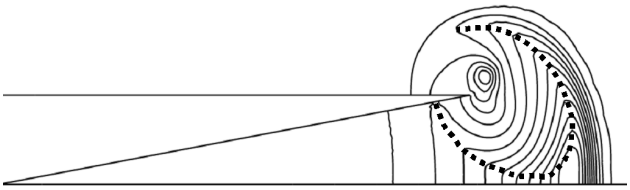

(c) 76 μs (t^* = 1.58)
(P_{max} = 2.67 atm, P_{min} = 0.440 atm, dP = 0.149 atm)
Fig. 9 Pressure contours (α_d = 10°)

exhaust is dominant until t^*_3. t^*_3 is almost equal regardless of α_d. After t^*_3, the refill takes over the exhaust. The duration of the refilling phase, i.e. $t^*_4 - t^*_3$, decreases with smaller α_d as in Fig. 8. Hence, the refill becomes active with the decrease in α_d. After t^*_4, C_m recovers significantly in the case of α_d = 10° due to fast refill, but is almost invariant in the case of α_d = 70° due to slow refill.

Flowfield in the refilling process

Figure 9 shows sequential pressure contours after shock wave has exited the nozzle. With smaller α_d, the shock wave expands rapidly from the nozzle exit. Thereby, a strong expansion wave propagates in the direction of central axis. This expansion wave lowers the pressure inside of nozzle and promotes following refill. This is illustrated in the figure. The broken line is the front of the expansion wave.

Same phenomenon occurs in the case of larger α_d. However, the expansion wave of larger α_d is weaker than that of smaller α_d because the expansion effect at the nozzle exit is small as shown in Fig. 10. The pressure drop is more moderate in the case of larger α_d. Therefore, in the case of larger α_d, pressure gradient between nozzle inside and outside is more gradual and it takes more time for refilling.

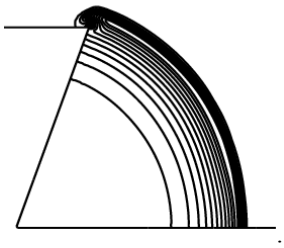

(a) 16 μs (t^* = 1.23)
(P_{max} = 3.56 atm, P_{min} = 0.709 atm, dP = 0.190 atm)

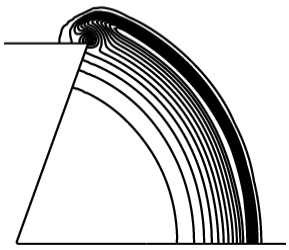

(b) 18 μs (t^* = 1.38)
(P_{max} = 3.18 atm, P_{min} = 0.688 atm, dP = 0.166 atm)

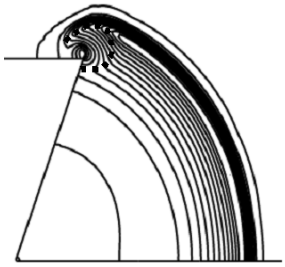

(c) 20 μs (t^* = 1.54)
(P_{max} = 2.90 atm, P_{min} = 0.712 atm, dP = 0.146 atm)
Fig. 10 Propagation of expansion wave (α_d = 70°)

Discrepancy between CFD and experiment

As previously seen in Fig. 6, the measured C_m is somewhat smaller than the CFD prediction, and the discrepancy becomes larger with α_d.

This would be due to the source model used in the calculation. As mentioned above, the center of source was set in the vicinity of cone apex. However, the pulse width of the CO_2 laser used in the experiment is 3μs and the center of explosion is approximately 10mm downstream of the laser focus, as shown in Fig. 11. This is because a laser supported detonation wave propagates during the laser heating.[1)]

Figure 12 shows the geometries of the blast wave in the experiment when the laser heating is terminated. In the case of α_d = 10° the nozzle scale is much larger than the propagation distance of a LSD wave. However, in the case of α_d = 70°, the LSD wave has

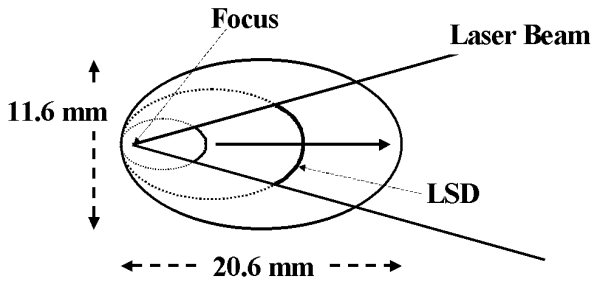

Fig. 11 The shape of the blast wave when the laser heating is terminated.

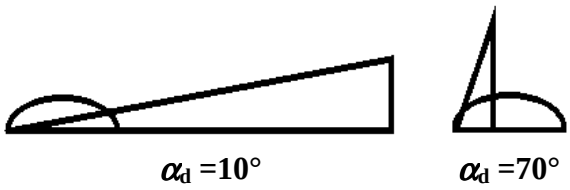

Fig. 12 Comparison of nozzle scale and source for r = 0.402

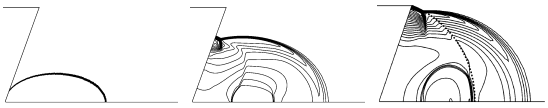

(a) A source model similar to the experimental condition (Computed C_m is 99 N/MW.)

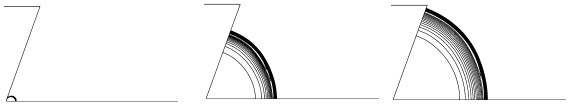

(b) Conventional source model condition (Computed C_m is 148 N/MW.)

Fig. 13 Influence of the source geometry (α_d = 70°)

propagated far from the nozzle exit. After the LSD wave exits from the nozzle, the subsequently absorbed energy doesn't contribute to thrust work. Thereby energy loss becomes large in the case of small nozzle scale.

Figure 13 shows the influence of source geometry on pressure contours. As shown in Fig. 13(a), the blast wave in the right side of broken line doesn't contribute to thrust. Computed C_m is 99 N/MW, which is about two third of the one with the conventional source model (Fig. 13(b)). However, it is still twice as large as the measured one.

To avoid this loss, laser pulse width should be so short that the propagation distance of the LSD wave can be smaller than the optimum nozzle length $R_{n,opt}=r_{opt}R^*$.

CONCLUSIONS

An optimum nozzle length was obtained. The optimum length is $0.3 \sim 0.4R^*$ regardless of the nozzle apex angle.

In addition, higher C_m was obtained with smaller apex angle. This is because a strong expansion wave propagates in the direction of central axis and this expansion wave lowers the pressure inside of nozzle more quickly in the case of smaller apex angle.

However, there found some discrepancies between the CFD predictions and measurements. This is partly because of the finite propagation period of a Laser Supported Detonation wave. To utilize the absorbed energy in the LSD process effectively, laser pulse width has to be short enough.

REFERENCES

[1] Mori, K., Komurasaki, K., and Arakawa, Y., J. Appl. Phys. **92**, 10, 2002

[2] Mori, K., Katsurayama, H., Hirooka, Y., Komurasaki K., and Arakawa, Y.: An Experimental Study on the Energy Balance in the Repetitively Pulsed Laser Propulsion, AIAA 2003-496.

[3] Wada, Y., and Liou, M.S.: A Flux Spliting Scheme With High-Resolution and Robustness for Discontinuities, NASA Technical Memorandum 106452 ICOMP-93-50, AIAA 94-0083.

[4] Edwards, J.R.: A Low-Diffusion Flux-Splitting Scheme for Navier-Stokes Calculations, Computers Fluids, 26, pp635-659, 1997

[5] Jameson A., and Yoon, S.: Lower-Upper Implicit Schemes with Multiple Grids for the Euler Equations, AIAA Journal, 25, pp929-935, 1987

[6] Matsuno, K.: Actual Numerical Accuracy of an Iterative Scheme for Solving for Solving Evolution Equations with Application to Boundary-Layer Flow, Trans. Japan Soc. Aero. Space. Sci., 38, pp.311-322, 1996

[7] Ritzel, D.V., and Matthews, K.: An adjustable explosion-source model for CFD blast calculations, Proc. Of 21st International Symposium on Shock Waves, pp.97-102, 1997

[8] Raizer, Y.P.: Laser-Induced Discharge Phenomena Studies in Soviet Science, Consultants Bureau, New York and London, 1977.